Fluctuation effects in first-order phase transitions: Theory and model for martensitic transformations

Per-Anker Lindgård
Physics Department, Risø National Laboratory, DK-4000 Roskilde, Denmark

Ole G. Mouritsen
Department of Structural Properties of Materials, The Technical University of Denmark, Building 307, DK-2800 Lyngby, Denmark

(Received 30 June 1989)

We discuss central questions in weak, first-order structural transitions by means of a magnetic analog model. A theory including fluctuation effects is developed for the model, showing a dynamical response with softening, fading modes and a growing central peak. The model is also analyzed by a two-dimensional Monte Carlo simulation, showing clear precursor phenomena near the first-order transition and spontaneous nucleation. The kinetics of the domain growth is studied and found to be exceedingly slow. The results are applicable for martensitic transformations and structural surface-reconstructive transitions.

I. INTRODUCTION

Many crystals, metallic or insulating, that at low temperatures have closed packed structures, undergo before melting a structural transformation to the more open body-centered-cubic (bcc) structure. This is called a martensitic transformation.[1] It is displacive in the sense that the atoms in the low-temperature unit cell are relocated into high-symmetry positions by finite displacements, with no exchange of atoms between cells, i.e., no diffusion. In spite of its universality and technological importance, the understanding of the underlying mechanism and the transformation process is still incomplete and the subject of vivid discussion.[2] Open questions are, for example: why is there no soft mode, is there a central peak, are there precursor effects, and are impurities necessary for nucleation or is it a spontaneous transition? We shall present here the results of a study that gives an answer to these questions for a model system of a martensitic transformation. Some of these results were briefly described previously.[3] Recently, it has been possible from first principles to calculate[4] the free energies of the transforming structures for actual materials, and thereby shed light on the thermodynamic driving forces, and the relevance of entropy, soft modes, strains, etc. For a high-temperature transition, this has so far only been done for the (hcp)↔(bcc) transition in Zr at 1140 K, with results in very satisfactory agreement with experimental measurements.[5] The temperature effects were calculated using anharmonic phonon theory. Since the atomic displacements of the order of the unit-cell dimension are large, the application of the small amplitude phonon theory is not fully satisfactory and cannot be used to discuss an important question such as nucleation.

Here we take a different approach and sacrifice the detailed description of a particular material for a principal phenomenological discussion of the physics involved in the martensitic transformation. Let us focus on the low-energy path an atom takes between the two structures. In coordinate space the path can be considered to be on a surface, and an atom on the path will feel large restoring forces perpendicular to the surface, while being able to perform large-amplitude fluctuations on the surface, largest along the path. In this picture the atoms may be thought of as the mass points of interacting pendulums, swinging in anisotropic potentials. They are attached to an imaginary reference lattice. If we now replace the pendulums by continuous spin variables, we are led to a magnetic analog model of the martensitic transformation which contains the principal dynamics and statistics of the atomic displacements. The advantage of the magnetic analogic model is that theories are developed[6] to describe large-amplitude vibrations, making it possible to describe temperature renormalization, soft modes, central peak and line-shape effects more reliably than by anharmonic, small-amplitude theory. Further, the magnetic model is suitable for computer simulation, and the thermodynamic phase diagram and important aspects like nucleation and domain growth kinetics can be studied with available computer resources. The advantage of using continuous spin variables, versus discrete Potts or Ising variables as in the axial next-nearest-neighbor interaction (ANNNI) model,[7] is that the former describe the statistical behavior, as well as the dynamics which the latter do not. Pseudospin models have previously been used for structural phase transitions.[8] Although we have used the magnetic analog model, discussed in this paper, for the martensitic transformation, it should be noted that the general results will be applicable to a large class of other transitions including surface reconstruction,[9] and transitions in metallurgy,[10] and earth science.[11]

In the following we first discuss the construction of magnetic analog models for the martensitic transformation. The properties obtained by the mean-field theory is

then discussed, prior to a discussion by means of a correlation theory of the excitation spectrum, the free energies and the line shape. Subsequently, the model is investigated by the Monte Carlo computer simulation method.

II. MODEL HAMILTONIANS FOR THE MARTENSITIC TRANSFORMATION

In order to understand the physics and statistical mechanics of the martensitic transformation in detail, it is advantageous to consider simple models which are tractable for numerical simulation and theoretical studies. There are several possible ways in which a bcc structure can transform to a closed-packed (cp) structure. Let us here consider the transformation shown in Fig. 1 in which, by moving all atoms in neighboring planes by an internal strain ϵ_2, it is possible to go from the bcc to the hcp or fcc structures with a certain relation between the symmetry axis in the different structures. This model is called the shuffling model and corresponds to the Nishiyama-Wasserman rule[1] for the bcc→fcc transition. The conserved planes are $(110)_{bcc}\rightarrow(111)_{fcc}$ or $(0001)_{hcp}$ and directions $[1\bar{1}0]_{bcc}\rightarrow[1\bar{2}1]_{fcc}$ or $[1\bar{1}00]_{hcp}$. In order to complete the closed-packed symmetry a uniform strain ϵ_1 is also needed along $z=(001)_{bcc}$ perpendicular to the conserved plane in order to reduce the angle $\theta_c=125.3°$ to $\theta_h=120°$. Considering a projection of the structure along the $[001]_{bcc}$ direction, the rearrangement can be depicted as a transformation in two dimensions between a square lattice to a triangular lattice, where the latter represents both the hcp and fcc phases. This is shown in the lower part of Fig. 1. The movements can equivalently occur either in the $\pm x$ or $\pm y$ direction and therefore give

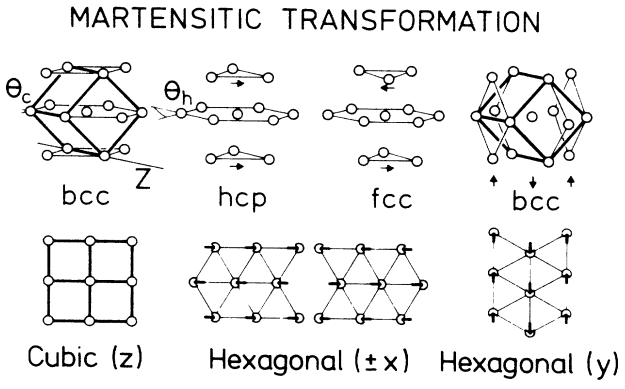

FIG. 1. A simple picture of the atomic displacements in a martensitic transformation. At the top left is shown a three-dimensional representation of a bcc structure, including some next-nearest neighbors connected with thin lines. The orientation is chosen such that it is evident that a shuffling of the horizontal planes as indicated by the arrows, leads to the closed packed hcp or fcc structures, after a further small adjustment of the angle $\theta_c\rightarrow\theta_h=120°$ by a uniform compression along the z axis. The top right shows that one could equivalently shuffle vertical planes. The lower part shows the same situation in a projection along the bcc (001) z axis. This reduces the problem, effectively, to a two-dimensional spin problem, representing the displacements by spins.

an order parameter of dimensionality $n=2$ and degeneracy $n_d=4$. It should be noted that for the real, structural bcc→cp transition there are three equivalents $(110)_{bcc}$ planes, out of which we by the projection have chosen one. The real bcc→cp transformation therefore has an order parameter with a degeneracy corresponding to $n_d=12$. Although the value of n does influence the critical behavior of the transition, we expect that the $n=2$ model contains the essential physics of the martensitic transformation. For a further simplification of the statistical mechanics of the atomic displacements depicted by arrows, we represent the atomic positions in the unit cells by actual spin $\mathbf{S}_i=(S_i^x,S_i^y,S_i^z)$ on a square reference lattice, where $\hat{\mathbf{r}}_{ij}$ represents a vector connecting nearest-neighbor spins $\mathbf{S}_i$ and $\mathbf{S}_j$. The physical content of this replacement will be discussed further in the following. The triangular lattices then correspond to antiferromagnetic structures with the ordered moments along either the x or y directions and the square lattice corresponds to a ferromagnetic structure with the moment along the z direction. We thus arrive at the magnetic Hamiltonian[3]

$$\mathcal{H}=\sum_{ij}\{J[\mathbf{S}_i\cdot\mathbf{S}_j-2(\hat{\mathbf{r}}_{ij}\cdot\mathbf{S}_i)(\hat{\mathbf{r}}_{ij}\cdot\mathbf{S}_j)] -KS_i^zS_j^z\}-P\sum_i(S_{ix}^4+S_{iy}^4)\ , \tag{1}$$

which at low temperatures for large K has the required ferromagnetic structure (called cubic z or phase 1), and for large J the required antiferromagnetic structure (called hexagonal x, y, or phase 2), the parameter $P>0$ stabilizes the x or y directions in the plane. We have used $P=2J$. There is a first-order transition between the cubic and hexagonal structures for a temperature-dependent ratio between K and J. For fixed K/J, the transition temperature T_M corresponds to the martensitic transformation temperature. At higher temperatures the model Eq. (1), of course, also has transitions to the paramagnetic phase (corresponding to melting in the real case), but this will not be of primary concern in this context. The model Eq. (1) for classical spins ($S=\infty$) is well suited for numerical simulations. For a theoretical investigation it is advantageous to consider a quantum mechanical $S=1$ model for which a theory for correlation effects has been developed.[6] For $S=1$ the P term in Eq. (1) can be written exactly in terms of tensor operators as

$$P(S_x^4+S_y^4)=P(\tfrac{1}{4}O_4^4+\tfrac{3}{140}O_4^0-S_z^2+1)\quad\text{for } S=1\ . \tag{2}$$

Since tensor operators O_l^m with $l=4$ do not have finite matrix elements for $S=1$, these can be neglected. So for $S=1$ the Hamiltonian Eq. (1) maps exactly onto the simpler one

$$\mathcal{H}=-\sum_{ij}\{J[\mathbf{S}_i\cdot\mathbf{S}_j-2(\hat{\mathbf{r}}_{ij}\cdot\mathbf{S}_i)(\hat{\mathbf{r}}_{ij}\cdot\mathbf{S}_j)] -KS_i^zS_j^z\}+D\sum_i S_{iz}^2\ . \tag{3}$$

Here the D term with $D=P=2J$ tends to stabilize the spins into the xy plane, but without preferring any specific directions; further, it introduces a singlet ground-state aspect into the problem. The dimensionali-

ty of the order parameter in the triangular phase is still $n=2$, but with continuous degeneracy. The model Eq. (3) is suitable for calculations using the correlation theory, but less so for numerical studies.

The advantage of using spin variables to describe the atomic motion, rather than the more conventional phonon variables, is that theories exist for describing large-amplitude spin vibrations, corresponding to large-amplitude atomic displacements. Phonon theory is basically only applicable for small-amplitude displacements. Previously,[7,8] it has been common to use Ising spin variables, such as in the ANNNI model, but then the dynamics of the transition cannot be described. The models Eqs. (1) and (3) are more appropriate for a dynamical description. This will be discussed in more detail in Sec. IV C.

III. MEAN-FIELD THEORY FOR THE MARTENSITIC TRANSFORMATION

In order to discuss the first-order transition between the cubic and the hexagonal phases, in the following indexed by 1 and 2, respectively, we need to calculate and compare the corresponding free energies $F_1(T)$ and $F_2(T)$. In mean-field (MF) theory the difference is

$$\Delta F=F_1-F_2=-k_BT\ln\left[\frac{\mathrm{Tr}e^{-\beta\mathcal{H}_1}}{\mathrm{Tr}e^{-\beta\mathcal{H}_2}}\right], \tag{4}$$

where $\beta=1/k_BT$. The mean-field Hamiltonians for the two structures are for Eq. (3)

$$\begin{aligned}\mathcal{H}_1&=2KM_1^2+\sum_i(DS_{iz}^2-H_1S_{iz}),\\ \mathcal{H}_2&=2JM_2^2+\sum_i(DS_{iz}^2-H_2S_{ix}),\end{aligned} \tag{5}$$

where the molecular fields are

$$H_1=(H_\parallel+4KM_1),\quad H_2=(H_1+4JM_2), \tag{6}$$

including an external uniform field $H_\parallel$ or staggered field $H_\perp$, and M_1 and M_2 are the order parameters. Diagonalizing Eq. (5) gives the eigenvalues and eigenfunctions tabulated in Table I, which yields the thermodynamic properties from the definitions of the partition function

$$Z_p=\sum_n\exp(-\beta E_p^{(n)}),\quad p=1,2,$$

and free energy

$$F_p=E_p^0-k_BT\ln Z_p,$$

where E_p^0 is the first term in Eq. (5). The corresponding classical expressions are obtained by replacing the sum by an integral giving

$$Z_p(\text{classical})=\int_0^{2\pi}\exp[-\beta\mathcal{H}_p(\theta)]d\theta$$

with $S_z=\cos\theta$ and $S_x=\sin\theta$ in $\mathcal{H}_p(\theta)$, cf. Eq. (5). The models can easily be examined analytically in the limits $T\to0$ and at $T\sim T_c$, where the magnetization is small.

Consider first $T=0$. The free energy reduces to $F_p=\langle\mathcal{H}\rangle_{p,T}=0$. For the classical case this gives directly

$$F_1=-2K+D,\quad F_2=-2J\quad(\text{classical},\ T=0). \tag{7}$$

For $D=2J$ the phase transition is therefore at $K/J=2$. The transition is of first order since F_1 and F_2 meet with a different slope as a function of K/J at $K/J=2$. For the $S=1$ case, F_p equals E_p^0 plus the lowest eigenvalue, and we find from Table I at $T=0$ the following:

$$\begin{aligned}&M_1=1,\quad M_2^2=1-(D/8J)^2=\tfrac{15}{16}\\ &F_1=2K+D-4K,\quad F_2=2JM_2^2+D/2-\Delta=-9J/8.\end{aligned}\qquad(S=1,T=0) \tag{8}$$

TABLE I. Mean-field eigenvalues $E_p^{(n)}$ and wave functions $\Psi_p^{(n)}$. The eigenfunctions for S_z are denoted $|0\rangle$ and $|\pm1\rangle$ and $|x\rangle=(|1\rangle+|-1\rangle)\sqrt{2}$, with $\langle0|S_x|x\rangle=1$. The mixing angle is given by $\sin2\Phi=H_2/\Delta$. The partition function Z_p, free energy F_p and magnetization M_p follow directly from the definitions. Finally the internal fields H_p are listed.

	Case $p=1$ (cubic)		Case $p=2$ (hexagonal)	
n	$E_1^{(n)}$	$\Psi_1^{(n)}$	$E_2^{(n)}$	$\Psi_2^{(n)}$
1	$D-H_1$	$\|1\rangle$	$D/2-\Delta$, $\Delta=\frac{1}{2}(D^2+4H_2^2)^{1/2}$	$\cos\Phi\|0\rangle+\sin\Phi\|x\rangle$
2	0	$\|0\rangle$	D	$(\|1\rangle-\|-1\rangle)/\sqrt{2}$
3	$D+H_1$	$\|-1\rangle$	$D/2+\Delta$	$\cos\Phi\|x\rangle-\sin\Phi\|0\rangle$
Z_p	$1+e^{-\beta D}(e^{\beta H_1}+e^{-\beta H_1})$		$e^{-\beta D}+e^{-\beta D/2}(e^{\beta\Delta}+e^{-\beta\Delta})$	
F_p	$2KM_1^2-k_BT\ln Z_1$		$2JM_2^2-k_BT\ln Z_2$	
M_p	$e^{-\beta D}(e^{\beta H_1}-e^{-\beta H_1})/Z_1$		$(H_2/\Delta)e^{-\beta D/2}(e^{\beta\Delta}-e^{-\beta\Delta})/Z_2$	
H_p	$4KM_1$		$4JM_2$	

This gives a first-order phase transition at $K/J=\frac{25}{16}=1.56$. If, as is often the case, the anisotropy had been included only as a linear effect, i.e., neglecting terms of order $(D/8J)^2$ and assuming $M_2=1$, one would obtain the first-order transition at $K/J=\frac{3}{2}$ at $T=0$.

Consider then $T\sim T_c$. For the $S=1$ case one finds from Table I by expanding for small M_p the local susceptibilities in the disordered phase for ordering in the z or x directions.

$$\chi_0^{zz}=\frac{2}{k_BT}\frac{\alpha}{1+2\alpha},\quad \chi_0^{xx}=\frac{2}{D}\frac{1-\alpha}{1+2\alpha}\ , \tag{9}$$

where $\alpha=\exp(-\beta D)$. These formulas were first derived by Van Vleck.[12] A second-order phase transition takes place when the inverse, interacting susceptibility vanishes

$$1/\chi_1=1/\chi_0^{zz}-4K,\quad 1/\chi_2=1/\chi_0^{xx}-4J\ . \tag{10}$$

The ordering of the antiferromagnetic x phase occurs at $1/\chi_2=0$, which for $D=2J$ gives

$$(1+2\alpha)/(1-\alpha)=4$$

or

$$\alpha=\tfrac{1}{2}\ .$$

From this, the (exact) MF-transition temperature is found to be

$$k_BT_c=2J/\ln(2)=2.89J\ .$$

The z order occurs at $1/\chi_1=0$ and is favorable for $K/J\geq 1/\ln(2)=1.44$. This is less than the ratio $K/J=1.56$ found at $T=0$. The phase transition between the ordered phases is obtained by a numerical calculation; see Fig. 2. If, as is often the case, one uses the linear high-temperature expansion giving

$$1/\chi_0^{zz}=3k_BT/2+D/2$$

and

$$1/\chi_0^{xx}=3k_BT/2-D\ ,$$

the bicritical point is found at $k_BT_c=3J$ and $K/J=\frac{3}{2}$, i.e., the same ratio as at $T=0$. In the linear approximation the critical ratio $K/J=\frac{3}{2}$ is independent of temperature, and there is no (martensitic) transformation as a function of temperature. We emphasize the fatal sensitivity of the phase diagram to fairly standard theoretical linearization approximations. In the next section we shall see that the same sensitivity holds true for the calculation of the excitation spectrum. For the classical case the expansion and integration of the partition function can be done, but is a bit cumbersome, so the total MF-phase diagram is calculated numerically for the full Hamiltonian Eq. (1); see Fig. 2. This can be compared with the result of the Monte Carlo simulation (dashed line), which includes correlation effects.

In order to discuss the correlation effects theoretically we need to calculate the excitation spectrum for the models. We will do this explicitly for the $S=1$ model. For this purpose it is appropriate to reformulate the Hamiltonian Eq. (3) into a more general form, which has been discussed previously.[6] As demonstrated above, conventional linearization procedures lead to incorrect results. Similarly it will be demonstrated that conventional linear spin-wave theory[13] is inadequate. Instead we shall use a theory[6] that allows a consistent treatment of correlation effects.

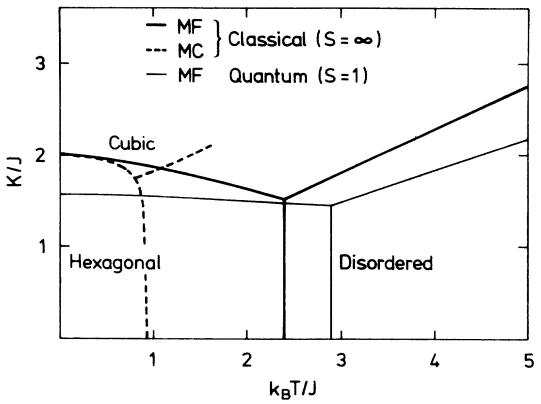

FIG. 2. Phase diagram showing a traditional bicritical point for the classical spin Hamiltonian Eq. (1) using mean-field theory and Monte Carlo simulation. Also shown is the mean-field phase digram for the quantum ($S=1$) model Eq. (3). A martensitic transformation corresponds to a crossing of the first-order line between the cubic and hexagonal phases as a function of temperature at a given ratio K/J.

IV. THE EXCITATATION SPECTRUM

A. Two-sublattice Hamiltonian

In order to develop the correlation theory for the excitation spectrum it is convenient to consider two sublattices, A and B, and rewrite the Hamiltonian Eq. (3) in the following general form, which has previously been studied[6]

$$\mathcal{H}=\mathcal{H}_{\rm int}+\mathcal{H}_{\rm an}=-\tfrac{1}{2}\sum_{ij}\sum_{\alpha}[\mathcal{J}_{ij}^{\alpha}(S_{iA}^{\alpha}S_{jA}^{\alpha}+S_{iB}^{\alpha}S_{jB}^{\alpha})+\mathcal{J}'^{\alpha}_{ij}(S_{iA}^{\alpha}S_{jB}^{\alpha}+S_{iB}^{\alpha}S_{jA}^{\alpha})]+\mathcal{H}_{\rm an}\ , \tag{11}$$

$$\mathcal{H}_{\rm an}=\sum_i\sum_{a=A,B}(DS_{ia}^{z2}-H_{\parallel}S_{ia}^{z})-H_{\perp}\sum_i(S_{iA}^{x}-S_{iB}^{x})\ ,$$

where $\alpha=x,y,z$ are Cartesian components. We here explicitly include the uniform and staggered external fields, $H_{\parallel}$ in the z direction and $H_{\perp}$ in the x direction. It is further convenient to introduce the uniform and staggered Fourier transformed variables $U_{\mathbf{q}}^{\alpha}$ and $V_{\mathbf{q}}^{\alpha}$ as

$$U_{\mathbf{q}}^{\alpha}=\sqrt{1/2}(S_{\mathbf{q}A}^{\alpha}+S_{\mathbf{q}B}^{\alpha})\quad\text{and}\quad V_{\mathbf{q}}^{\alpha}=\sqrt{1/2}(S_{\mathbf{q}A}^{\alpha}-S_{\mathbf{q}B}^{\alpha})\ , \tag{12}$$

and the new interaction constants, $J_{\mathbf{q}}^{\alpha}=\mathcal{J}_{\mathbf{q}}^{\alpha}+\mathcal{J}'^{\alpha}_{\mathbf{q}}$ and $I_{\mathbf{q}}^{\alpha}=\mathcal{J}_{\mathbf{q}}^{\alpha}-\mathcal{J}'^{\alpha}_{\mathbf{q}}$. For the Hamiltonian Eq. (3) these are given explicitly for the two-dimensional lattice by

$$J_{\mathbf{q}}^{x}=-J_{\mathbf{q}}^{y}=J\gamma'_{\mathbf{q}},\quad J_{\mathbf{q}}^{z}=K\gamma_{\mathbf{q}}\ ,$$
$$I_{\mathbf{q}}^{x}=-I_{\mathbf{q}}^{y}=J\gamma_{\mathbf{q}},\quad I_{\mathbf{q}}^{z}=K\gamma'_{\mathbf{q}}\ , \tag{13}$$
$$\gamma_{\mathbf{q}}=2(\cos q_x+\cos q_y),\quad \gamma'_{\mathbf{q}}=2(\cos q_x-\cos q_y)\ .$$

In terms of the variables, Eq. (12), the pair interaction, first term in Eq. (11), is diagonalized with respect to the sublattices and becomes

$$\mathcal{H}_{\rm int}=-\tfrac{1}{2}\sum_{\mathbf{q}\alpha}(J_{\mathbf{q}}^{\alpha}U_{\mathbf{q}}^{\alpha}U_{-\mathbf{q}}^{\alpha}+I_{\mathbf{q}}^{\alpha}V_{\mathbf{q}}^{\alpha}V_{-\mathbf{q}}^{\alpha})\ . \tag{14}$$

The advantage of this procedure is that the uniform and staggered modes can then be discussed. We now define the following quadrupolar operators for each sublattice:

$$\hat{Q}_x=2(S_z^2-S_y^2),\quad \hat{Q}_y=2(S_z^2-S_x^2)\ ,$$
$$\hat{Q}_z=2(S_x^2-S_y^2),\quad L^x=(S^zS^y+S^yS^z)\ , \tag{15}$$

with the remaining L^{α} obtained by cyclic permutations. These operators are needed in order to treat the anisotropy term correctly. With indices u and v we indicate the linear combinations corresponding to Eq. (12).

Commutators between spin and quadrupolar operators give again quadrupolar operators, and commutators between two quadrupolar operators give spin operators for $S=1$. These are derived from the definitions Eqs. (12) and (15).

B. Summary of the general correlation theory

The idea of the correlation theory is to calculate both the static and dynamic properties self-consistently, including correlation effects in a mode-mode coupling approximation. The theory has previously been reviewed in detail,[6] so here we only give a few basic steps. First a dynamical vector variable $\underline{A}_q$ is constructed consisting of a relevant number of the operators Eqs. (12) and (15). For $\underline{A}_q$ the exact first- and second-order equations of motion can, by separating out all terms proportional to $\underline{A}_{\mathbf{q}}$, be written as

$$i\dot{\underline{A}}_{\mathbf{q}}=[\underline{A}_{\mathbf{q}},\mathcal{H}]=\langle\underline{\omega}_{\mathbf{q}}\rangle\underline{A}_{\mathbf{q}}+\underline{X}_{\mathbf{q}}\ , \tag{16}$$

$$-\ddot{\underline{A}}_{\mathbf{q}}=\langle\underline{\omega}_{\mathbf{q}}^2\rangle\underline{A}_{\mathbf{q}}+\underline{X}_{\mathbf{q}}^{(2)}\ , \tag{17}$$

$$\underline{\Delta}_{\mathbf{q}}^2=\langle\underline{\omega}_{\mathbf{q}}^2\rangle-\langle\underline{\omega}_{\mathbf{q}}\rangle^2\ , \tag{18}$$

Here $\underline{X}_{\mathbf{q}}$ and $\underline{X}_{\mathbf{q}}^{(2)}$ are so-called random forces, not proportional to $\underline{A}_{\mathbf{q}}$. $\langle\underline{\omega}_{\mathbf{q}}^n\rangle$ are the frequency moments of the relaxation function $(\underline{A}_{\mathbf{q}}\underline{A}_{\mathbf{q}}^{\dagger})_{\omega}$. If $\underline{\Delta}_{\mathbf{q}}^2$ is nonzero, it directly tells us that the spectrum does not consist of δ functions, but the excitations have a finite linewidth. Next, since $i(\dot{\underline{A}}\underline{B}^{\dagger})=\langle[\underline{A},\underline{B}^{\dagger}]\rangle$ one can from Eq. (16) derive the exact relation

$$\underline{\chi}_{\mathbf{q}}=\langle\underline{\omega}_{\mathbf{q}}\rangle^{-1}\underline{I},\quad \langle\underline{\omega}_{\mathbf{q}}\rangle=\underline{I}\underline{\chi}_{\mathbf{q}}^{-1}\ , \tag{19}$$
$$\underline{I}=\langle[\underline{A}_{\mathbf{q}},\underline{A}_{\mathbf{q}}^{\dagger}]\rangle\ . \tag{20}$$

We emphasize this important exact result, that the susceptibility is inversely proportional to the first frequency moment and vice versa. The matrix $\underline{I}$ only involves thermal averages of single-site operators. Similarly using Eq. (17) we can alternatively, and still exactly, write

$$\underline{\chi}_{\mathbf{q}}=\underline{\Delta}_{\mathbf{q}}^{-2}\underline{\rho}_{\mathbf{q}}\ ,\quad \langle\underline{\omega}_{\mathbf{q}}\rangle=\underline{I}\underline{\rho}_{\mathbf{q}}^{-1}\underline{\Delta}_{\mathbf{q}}^2\ , \tag{21}$$
$$\underline{\rho}_{\mathbf{q}}=\langle[\underline{X}_{\mathbf{q}},\underline{A}_{\mathbf{q}}^{\dagger}]\rangle\ . \tag{22}$$

The advantage of using the second derivative Eq. (17) for defining the susceptibility is that it includes explicitly the average of the time-dependent variations of the neighborhood of the operator we are dealing with. Therefore correlation with the neighborhood is explicitly involved. Using Eq. (19) all these correlation effects are hidden in the thermal single-site averages. Equation (21) is a useful starting point for approximations. Likewise is the following exact formal solution by Mori[14] for the frequency dependence of the Laplace transformed dynamical relaxation function. Let us summarize a number of exact results:

$$(\underline{A}_{\mathbf{q}}\underline{A}_{\mathbf{q}}^{\dagger})_z=\underline{\chi}_{\mathbf{q}}[z\underline{1}-i\underline{\Omega}_{\mathbf{q}}+\underline{\Sigma}_{\mathbf{q}}(z)]^{-1}\ ,$$
$$\underline{\Sigma}_{\mathbf{q}}(z)=(\underline{X}_{\mathbf{q}}\underline{X}_{\mathbf{q}}^{\dagger})_z\underline{\chi}_{\mathbf{q}}^{-1}\ ,$$
$$(\underline{A}_{\mathbf{q}}\underline{A}_{\mathbf{q}}^{\dagger})_{\omega}=\mathrm{Re}(\underline{A}_{\mathbf{q}}\underline{A}_{\mathbf{q}}^{\dagger})_{z=i\omega}\ , \tag{23}$$
$$\langle\underline{A}_{\mathbf{q}}\underline{A}_{\mathbf{q}}^{\dagger}\rangle=\int_{-\infty}^{\infty}(\underline{A}_{\mathbf{q}}\underline{A}_{\mathbf{q}}^{\dagger})_{\omega}/(1-e^{-\beta\omega})\omega\,d\omega\ ,$$
$$\langle\underline{\omega}_{\mathbf{q}}^n\rangle=\int_{-\infty}^{\infty}\omega^n(\underline{A}_{\mathbf{q}}\underline{A}_{\mathbf{q}}^{\dagger})_{\omega}d\omega\,\underline{\chi}_{\mathbf{q}}^{-1}\ .$$

The relation to the frequency-dependent relaxation function and the static correlation functions is also given. This completes the description of the formally exact theory. The approximation made in the correlation theory[6] consists of the following three assumptions: (a) that the effects of the remaining operator $\underline{X}_{\mathbf{q}}^{(2)}$ in Eq. (17) can be neglected, (b) that the terms in $\dot{\underline{A}}_{\mathbf{q}}$ Eq. (16) proportional to $\underline{A}_{\mathbf{q}}$ obtained by the random-phase approximation (RPA) decoupling, and the terms in $\ddot{\underline{A}}_{\mathbf{q}}$ (17) proportional to $\underline{A}_{\mathbf{q}}$, obtained by a mode-mode decoupling of all triple products of operators like

$$ABC\sim\langle AB\rangle C+\langle AC\rangle B+\langle BC\rangle A\ ,$$

are sufficiently close to the exact projections so we can use the Mori result Eq. (23), and finally (c) the dynamical assumption that the frequency dependence of the second-order random force relaxation function is unimportant in the frequency range of interest. Let us now apply this theory to the two specific cases.

C. RPA theory of "cubic" excitations in the ferromagnetically z-ordered phase

Case 1 is the analog to the cubic phase, for which the order parameter and the molecular field are

$$M_1=\langle S_A^z+S_B^z\rangle/2=\langle U_0^z\rangle/\sqrt{2},\quad H_1=H_\parallel+J_0^zM_1\ , \tag{24}$$

and $H_\perp=0$. The theory is sufficiently general to also apply for the disordered phase for which $M_1=H_1=0$. For the transverse excitations corresponding to S_q^x and S_q^y modes we need the dynamical variable vector

$$\underline{A}_q=\text{column}(U_q^x,L_{qu}^y,U_q^y,L_{qu}^x) \tag{25}$$

describing the uniform or acoustic modes, and similarly the V operators for the optic modes. The L_{qu}^α operators are generated by the equations of motion. The first moment matrix is directly found from Eq. (16) by a RPA decoupling of operators on different sites, for example,

$$\Sigma_k J_{k+q}^y U_{k+q}^y U_{-k}^z \sim J_q^y\langle U_0^z\rangle U_q^y\ .$$

Operators on the same site are treated exactly,

$$\langle\underline{\omega}_q\rangle=\frac{(\dot{\underline{A}}_q\underline{A}_q^\dagger)}{(\underline{A}_q\underline{A}_q^\dagger)}=i\begin{bmatrix}0&0&H_q^y&-D\\0&0&-D_q^y&H_1\\-H_q^x&D&0&0\\D_q^x&-H_1&0&0\end{bmatrix}\ . \tag{26}$$

We define the q-dependent field and anisotropy terms

$$H_q^\alpha=H_1-J_q^\alpha M_1,\quad D_q^\alpha=D-J_q^\alpha Q^\alpha\ , \tag{27}$$

and the squared frequencies

$$\omega_{qex}^2=H_q^xH_q^y,\quad \omega_{qD}^{\alpha2}=D(D-J_q^\alpha Q^\alpha)=DD_q^\alpha\ , \tag{28}$$

where $Q^\alpha=\langle\hat{Q}_\alpha\rangle$ from Eq. (15) and by symmetry $Q^x=Q^y$. Here ω_{qex} is the exchange frequency found in the absence of the anistropy D, and ω_{qD}^α is the exciton frequency found in the absence of magnetic order. The eigenvalues for Eq. (26) are the solutions to the determinant equation, which can be written

$$\begin{aligned}&\lambda_\pm^2=\tfrac{1}{2}\Omega^2[1\pm(1-4\omega_{qu1}^2/\Omega^2)^{1/2}]\ ,\\&\Omega^2=\omega_{qD}^{y2}+\omega_{qD}^{x2}+\omega_{qex}^2+H_1^2\ ,\\&\omega_{qu1}^2=(H_1H_q^x-\omega_{qD}^{x2})(H_1H_q^y-\omega_{qD}^{y2})/\Omega^2\ .\end{aligned} \tag{29}$$

If we neglect the transverse part of $\mathcal{H}_{int}$ Eq. (11), i.e., all J_q^x and J_q^y terms we get $\lambda_\pm^2=(D\pm H_1)^2$. This shows that λ_+ corresponds to resonances for transitions between the excited levels 2 and 3 in Table I. At temperatures where the order parameter M_1 is close to the saturation value (typically for $T\le 75\%\ T_c$) we can neglect the population of the excited level and thus the effect of the λ_+ resonance. The other eigenvalue λ_- corresponds to excitations between the ground state and the first excited state (1 and 2 in Table I). In the same temperature range we can expand λ_-^2 and find the low-frequency excitation $\lambda_-^2\simeq\omega_{qu1}^2$. This determines the RPA spin-wave frequency ω_{qu1} for case 1. In order to derive the susceptibility $\underline{\chi}_q$ from Eq. (19) we need the matrix $\underline{I}$, which can be directly found from (20):

$$\underline{I}=\langle[\underline{A}_q,\underline{A}_q^\dagger]\rangle=i\begin{bmatrix}0&0&M_1&-Q^x\\0&0&-Q^y&M_1\\-M_1&Q^y&0&0\\Q^x&-M_1&0&0\end{bmatrix}\ , \tag{30}$$

$$\underline{\chi}_q=\langle\underline{\omega}_q\rangle^{-1}\underline{I}\ . \tag{31}$$

Using Eq. (26) and (30), and the (1,1) and (3,3) elements of (31), the RPA susceptibilities for the uniform and staggered fields are

$$\begin{aligned}&\chi_{qu1}^\alpha=(U_q^\alpha U_q^{\alpha\dagger})=1/(R_1^\alpha-J_q^\alpha)\ ,\\&\chi_{qv1}^\alpha=(V_q^\alpha V_q^{\alpha\dagger})=1/(R_1^\alpha-I_q^\alpha)\ .\end{aligned} \tag{32}$$

The staggered susceptibility is obtained by analogy, using the result Eq. (14). The R_1^α term is the inverse local susceptibility, which is found to be

$$R_1^\alpha=1/\chi_0^{\alpha\alpha}=\frac{H_1^2-D^2}{H_1M_1-DQ^\alpha}\ . \tag{33}$$

If M_1 and Q^α are evaluated in the mean-field approximation, Eq. (33) agrees exactly with the directly calculated mean-field susceptibility, as given by the Van Vleck[12] formula for Eq. (9). This shows that the decoupling in the theory is exact, with respect to the single-site properties. Using Eqs. (33) and (27) we can reformulate ω_{qu1}^2 in Eq. (29) and find the more general expression for the spin-wave frequency for the uniform mode

$$\begin{aligned}\omega_{qu1}&=K_1M_1[(R_1^\alpha-J_q^x)(R_1^y-J_q^y)]^{1/2}\\&=K_1M_1/(\chi_{qu1}^x\chi_{qu1}^y)^{1/2}\ .\end{aligned} \tag{34}$$

For the staggered mode we replace J_q^α by I_q^α, and the index u by v, K_1 is a weakly q-dependent constant of order 1. This shows explicitly that the first moment frequency vanishes at the temperature at which χ_q^α diverges for some q, here at $q=0$, as expected from the general definition Eq. (19). Using the mean-field theory, Table I, at $T=0$ we find $M_1=1$, $Q^\alpha=-1$, and hence from Eq. (33)

$$R_1^\alpha=H_1-D=4K-2J\ .$$

Now $\chi_q^\alpha=0$ diverges for $R_1^\alpha-4J=0$ or for $K/J=\frac{3}{2}$. This ratio is lower than the ratio 1.56 found previously for the first-order transition. There is therefore no soft mode when approaching the transition from the z phase (or cubic phase). It is interesting, however, that the ratio is higher than the critical ratio $K/J=1.44$ at $T=T_c$. In the interval $1.44<K/J<1.5$ the model Eq. (3) represents a case for which the cubic order is not stable at low temperatures, but is stabilized at high temperatures by anharmonic effects. This was precisely the case found for the real martensitic transformation in Zr,[4] where the linear phonon theory for the potential, calculated from first principles, yielded imaginary frequencies at low temperatures. Whereas anharmonic phonon theory gave a

stable cubic phase at higher temperature, the anharmonic theory for phonons is very difficult and basically restricted to perturbation theory. For spin dynamics, which is inherently anharmonic, since the spin operators are infinite expansions of Bose operators,[13] theories like the correlation theory[6] are developed for dealing with such anharmonicity. The spin operators can be thought of as infinite expansions in Bose operators, which could be atomic displacement operators or phonon operators. Treating such appropriate infinite groups of operators consistently, allows a description of finite atomic displacements, and not just the infinitesimal displacements discussed by a linear phonon theory. In the martensitic transformation the involved displacements are within the atomic unit cell. The spin analogy, where the head of the spin represents the actual atomic position relative to a reference lattice, is therefore quite realistic. In this model the atomic large-amplitude displacements are confined to a sphere. Although this is probably too simplified, the description gives an approximation for the minimum energy path for the atoms between two structural positions, while neglecting any effect of small vibrations perpendicular to the surface for this path. In this picture it is also possible, physically, to understand the difference between the quantum and the classical model. The latter allows the atom to be anywhere on the globe. The quantum $S=1$ model prefers the atoms to jump from the poles ($S_z=\pm 1$), corresponding to the cubic positions, to the equatorial plane ($S_z=0$), corresponding to the hexagonal phase. This model may be more realistic than the classical one and also allows for tunneling effects. The minimum path and energy barrier between the $S_z=\pm 1$ and $S_z=0$ positions could be modeled more realistically by modifying the interaction and potential terms in Eqs. (1) and (3) if desired

It is interesting to compare Eq. (34) with the result of a harmonic, linear spin-wave theory using Bose operators a and $a^\dagger$ from a truncated Holstein-Primakoff (HP) transformation,[13] which replaces the spin operators as follows: $S^+=\sqrt{2S}\,a$, $S^-=\sqrt{2S}\,a^\dagger$, $S_z=S-a^\dagger a$, for large S. The familar result for Eq. (3) is

$$\omega_{qu1}=M_1\{[J_0^z-D(2S-1)-J_q^x] \times[J_0^z-D(2S-1)-J_q^y]\}^{1/2} . \tag{35}$$

This agrees with Eq. (34) for $S=1$. The limit for classical spins ($S\to\infty$) is obtained by replacing $2S-1$ by 2, the coefficient to the highest power of S. Now ω_{qu1} vanishes at

$$H_1-2D-J_0^x=4K-8J=0 ,$$

i.e., at $K/J=2$. The classical, harmonic spin-wave theory for Eq. (3), therefore, predicts a soft mode at the first-order transition at $K/J=2$ and similarly, when applied to the $S=1$ case, a soft mode at the *linear* first-order transition at $K/J=\frac{3}{2}$. On the other hand the P term in Eq. (1) can for classical spins be written

$$(S_x^4+S_y^4)=\tfrac{1}{4}O_4^4+\tfrac{3}{140}O_4^0-\tfrac{2}{7}O_2^0+\tfrac{2}{5} \sim\tfrac{1}{2}(a^{\dagger 4}+a^4)+\tfrac{18}{7}a^{\dagger 2}a^2 , \tag{36}$$

where the expansion to Bose operators is found using the large S limit of the well-ordered expansions of the O_l^0 operators[15] (direct HP transformation of $S_x^4+S_y^4$ leads to erroneous results). The P term Eq. (36) represents a strongly anharmonic term, which give no contribution in a simple harmonic theory. The spin-wave frequency ω_{qu1}, for Eq. (1), is hence given by an expression like Eq. (35) with $D=0$. This frequency is zero for $K/J=1$. For the classical case linear spin-wave theory for Eq. (1) therefore gives no soft mode at the first-order transition at $K/J=2$. Further, the cubic phase for Eq. (1) is inherently stable in the whole martensitic transformation interval $1.5<K/J<2$, see Fig. 2.

D. RPA theory of "hexagonal" excitations in the antiferromagnetically x-ordered phase

Case 2 is analogous to the closed-packed phase for which the order parameter and molecular field are

$$M_2=\langle S_A^x-S_B^x\rangle/2=\langle V_0^x\rangle/\sqrt{2},\quad H_2=H_\perp+I_0^xM_2$$

and $H_\parallel=0$. For the transverse excitations we need the dynamical variable vector

$$\underline{A}_q=\text{column}\,(U_q^y,\ L_{qv}^z,\ V_q^z,\ L_{qu}^y) . \tag{37}$$

The first moment matrix is

$$\langle\underline{\omega}_q\rangle=i\begin{bmatrix} 0 & 0 & H_q^z & D \\ 0 & 0 & D_q^z & H_2 \\ -H_q^y & 0 & 0 & 0 \\ -D_q^y & -H_2 & 0 & 0 \end{bmatrix} , \tag{38}$$

using the same notation as in Eq. (27), but with

$$D_q^z=-I_q^zQ^z ,$$

$$H_q^z=H_2-I_q^zM,\quad H_q^y=H_2-J_q^yM_2$$

and

$$\omega_{qex}^2=H_q^yH_q^z,\quad \omega_{qD}^{z2}=DD_q^z .$$

Here $Q^z=2\langle S_x^2-S_y^2\rangle$ from Eq. (15). The eigenvalues are solutions to the determinant equation giving results similar to Eq. (29). The spin-wave excitation from the ground state has now the squared frequency

$$\omega_{qu2}^2=H_2H_q^y(H_2H_q^z-\omega_{qD}^{z2})/(\omega_{qd}^{y2}+\omega_{qex}^2+H_2^2) .$$

The matrix $\underline{I}$ and the susceptibility in Eq. (19) are

$$\underline{I}=i\begin{bmatrix} 0 & 0 & M_2 & Q^y \\ 0 & 0 & Q^z & M_2 \\ -M_2 & -Q^z & 0 & 0 \\ -Q^y & -M_2 & 0 & 0 \end{bmatrix} , \tag{39}$$

$$\underline{\chi}_q=\langle\underline{\omega}_q\rangle^{-1}\underline{I} .$$

The (1,1) and (3,3) elements give the RPA susceptibilities

$$\chi^2_{qu2}=(U^y_q U^y_{-q})=\frac{1}{R^y_2-J^y_q},$$
$$\chi^z_{qv2}=(V^z_q V^z_{-q})=\frac{1}{R^z_2-I^z_q}, \tag{40}$$

where the local inverse susceptibilities are

$$R^y_2=1/\chi^{yy}_0=H_2/M_2=4J,$$
$$R^z_2=1/\chi^{zz}_0=H^2_2/(H_2M_2-DQ^z). \tag{41}$$

Again, if M_2 and Q^z are calculated using the mean-field theory, (41) agrees exactly with the directly calculated Van Vleck susceptibilities Eq. (9) and gives $R^z_2=\frac{1}{2}D$ at $T=0$. Similarly to Eq. (34) we can reformulate ω_{qu2} and the corresponding ω_{qv2} as

$$\omega_{qu2}=K_2M_2[(R^y_2-J^y_q)(R^z_2-I^z_q)]^{1/2}$$
$$=K_2M_2/(\chi^y_{qu2}\chi^z_{qv2})^{1/2}$$
$$\omega_{qv2}=K_2M_2[(R^y_2-I^y_q)(R^z_2-J^z_q)]^{1/2} \tag{42}$$
$$=K_2M_2/(\chi^y_{qv2}\chi^z_{qu2})^{1/2},$$

where K_2 is a weakly q-dependent constant of order 1. Using the mean-field theory, Table I, we find at $T=0$ for this case with $D=2J$ a reduced magnetization $M^2_2=\frac{15}{16}$ and $Q^z=-\frac{5}{4}$. The instability towards the z order occurs for $\chi^z_{qu2}\to 0$ or at $R^z_2=4$ K. This gives a stability range for the x order for $K/J<\frac{5}{3}=1.67$. This is higher than the ratio 1.56 found for the first-order transition. There is, therefore, no soft mode when approaching the transition from the x phase (or cubic phase) either.

The harmonic, linear spin-wave theory using the HP transformation gives

$$\omega_{q2}=M_2\{(I^x_0-I^y_q)[I^x_0+D(2S-1)-J^z_q]\}^{1/2}. \tag{43}$$

Since this includes only effects linear in D it does not agree with the RPA result Eq. (42) and a soft mode is obtained at $K/J=\frac{3}{2}$. The *linear theories* therefore predict soft modes when approaching the first-order transition at low temperatures from both phases. This shows first of all that the accuracy of standard linear theories is not sufficient for discussing a delicate phenomenon such as martensitic transformation. We expect that this statement also holds for the application of linear phonon theory.

The P term in (1) can, with x as the quantization axis, be written as[15]

$$P(S^y_x+S^y_y)=\tfrac{1}{8}O^4_4-\tfrac{1}{14}O^2_4+\tfrac{11}{280}O^0_4+\tfrac{3}{7}O^2_2+\tfrac{1}{7}O^0_2+\tfrac{2}{5}$$
$$\sim 1-4a^\dagger a+\tfrac{1}{8}(a^4+a^{\dagger 4}). \tag{44}$$

The spin-wave frequency ω_{qv2} for (1) is given by an expression like Eq. (43) with $D(2S-1)$ replaced by $4P$. This frequency is zero for $K/J=3$. Therefore, linear spin-wave theory for the classical Hamiltonian Eq. (1) gives no soft mode at the transition at $K/J=2$, when approaching it from neither the cubic-orderered nor the hexagonal-ordered phases.

E. Effect of fluctuations

In order to find the fluctuation effects on the first moment we use the result Eq. (21) and calculate and decouple the second-order equations of motion for the dynamical variable Eqs. (25) and (37). Both for the cubic and the hexagonal order we find that the $\underline{\rho}_q$ and $\underline{\Delta}^2_q$ matrices are diagonal with matrix elements for the spin operators of the general form

$$\rho_q=C_{q1},\quad \Delta^2_q=C_{q2}-C_{q1}J_q, \tag{45}$$

where C_{q1} and C_{q2} are correlation functions in various combinations and J_q is the interaction constants J^α_q or I^α_q. According to Eq. (21) one therefore finds the important result that the general RPA form for the enhanced susceptibility Eqs. (32) and (40), and furthermore the first moment frequencies Eqs. (34) and (42) are recovered, but the local susceptibilities $1/R^\alpha$ are replaced by renormalized, and in principle wave-vector-dependent susceptibilities $1/R^\alpha_q$, which depend on correlations within a small cluster. Explicitly for the cubic order we find that R^y_1 in Eq. (34) for the uniform (U) mode must be replaced by

$$R^x_1\to R^x_{qu1}=C^x_{qu2}/C^x_{qu1},$$
$$C^x_{qun}=\sum_k[(J^z_k-J^y_{k-q})J^{z(n-1)}_k\langle\delta U^z_k\delta U^z_{-k}\rangle$$
$$+(J^y_k-J^z_{k-q})J^{y(n-1)}_k\langle U^y_k U^y_{-k}\rangle \tag{46}$$
$$+(I^z_k-I^y_{k-q})I^{z(n-1)}_k\langle V^z_k V^z_{-k}\rangle$$
$$+(I^y_k-I^z_{k-q})I^{y(n-1)}_k\langle V^y_k V^y_{-k}\rangle],$$

where $\delta U^z_k=U^z_k-\langle U^z_0\rangle$ and $J^{(n-1)}$ is 1 and J for $n=1$ and 2, respectively. By symmetry, $R^x_{qu1}=R^y_{qu1}$. For the staggered mode, C^x_{qvn} is obtained from Eq. (46) when J^α_{k-q} is replaced by I^α_{k-q} and vice versa. In general, $R^\alpha_{qu1}\neq R^\alpha_{qv1}$. At low temperature the longitudinal (z) fluctuations can be neglected. Since $\Sigma_k J_k\langle S^\alpha_k S^\alpha_{-k}\rangle$ is a nearest-neighbor correlation function and $\Sigma_k J^2_k\langle S^\alpha_k S^\alpha_{-k}\rangle$ is a sum of an on-site and a next-nearest-neighbor correlation function, R^α_{qu1} and R^α_{qv1} are nonlocal inverse susceptibilities for a small cluster.

For the hexagonal order we similarly find that R^α_2 in ω_{qu2} in Eq. (42) must be replaced by

$$R^y_2\to R^y_{qu2}=C^y_{qu2}/C^y_{qu1},\quad R^z_2\to R^z_{qv2}=C^z_{qv2}/C^z_{qv1}, \tag{47}$$

where C^α_{qun} are obtained from Eq. (46) by cyclic permutations, and now δV^x_k is inserted instead of V^x_k but where now these longitudinal terms can be neglected at low temperatures.

Let us now evaluate the correlation functions using the aforementioned formulas and the general formula found in Eq. (23). In a quasiharmonic approximation we as-

sume that the spectrum can be represented by δ functions at the first moment frequency, i.e., we neglect the damping term $\Sigma_{\mathbf{q}}(z)$ in Eq. (23). The scattering function for the cases $p=1$ and 2 then assumes the form[6]

$$(U^{\alpha}_{\mathbf{q}}U^{\alpha}_{-\mathbf{q}})_{\omega p}=\chi^{\alpha}_{\mathbf{q}up}\tfrac{1}{2}[\delta(\omega-\omega_{\mathbf{q}up})+\delta(\omega+\omega_{\mathbf{q}up})]f_{\mathbf{q}up}\ , \tag{48}$$

where $f_{\mathbf{q}up}$ is a factor of order 1 when the order parameter is close to the saturation value (i.e., the upper mode at Ω can be neglected). Consequently, Eq. (23) can now be integrated over ω to yield the correlation function

$$\begin{aligned}&\langle U^{\alpha}_{\mathbf{q}}U^{\alpha}_{-\mathbf{q}}\rangle_p=\chi^{\alpha}_{\mathbf{q}up}\omega_{\mathbf{q}up}(n_{\mathbf{q}up}+\tfrac{1}{2})\\&n_{\mathbf{q}up}=1/[\exp(\omega_{\mathbf{q}up}/k_BT)-1]\ ,\end{aligned} \tag{49}$$

where $n_{\mathbf{q}up}$ is the spin-wave population factor for the U modes in phase p. At $T\to 0$ this vanishes and the correlation functions reduce to the value of the small quantum-mechanical zero-point motion effect. At T approaching the second-order transition, where the susceptibility diverges faster than the first moment frequency decreases, Eq. (49) shows that the transverse fluctuations diverge. This is also true when the upper mode at Ω is included. It is also clear that the most diverging correlations are those corresponding to the competing phase. (The discussion of the V modes is completely analogous.) As the potential second-order boundaries were found to be quite close to the first-order transition, we predict a substantial growth of the short-range order corresponding to the competing phase, when the first-order boundary is approached, be it as a function of temperature as in the martensitic transformation or by varying the parameters K and J.

We can now also calculate the free energies including the fluctuation effects. First we rewrite the thermal averages of Eq. (11) exactly as (for $H_{\parallel}=H_{\perp}=0$)

$$\begin{aligned}\langle\mathcal{H}\rangle_T=&-\tfrac{1}{2}\sum_{\mathbf{q}\alpha}(J^{\alpha}_{\mathbf{q}}\langle U^{\alpha}_{\mathbf{q}}U^{\alpha}_{-\mathbf{q}}\rangle+I^{\alpha}_{\mathbf{q}}\langle V^{\alpha}_{\mathbf{q}}V^{\alpha}_{-\mathbf{q}}\rangle)\\&+D\sum_{\mathbf{q}}(\langle U^{z}_{\mathbf{q}}U^{z}_{-\mathbf{q}}\rangle+\langle V^{z}_{\mathbf{q}}V^{z}_{-\mathbf{q}}\rangle)\ .\end{aligned} \tag{50}$$

The free energy can be exactly written as[16]

$$F=\langle\mathcal{H}\rangle_T-T\mathcal{S}=\langle\mathcal{H}\rangle_{T=0}-T\int_0(\langle\mathcal{H}\rangle_{T'}-\langle\mathcal{H}\rangle_{T'=0})\frac{dT'}{T'^2}\ . \tag{51}$$

Using Eq. (49), and assuming the temperature variation is dominated by the population factor, Eq. (51) can be integrated and written as

$$F_p=E_p(T)+E_p^0+k_BT\tfrac{1}{2}\sum_{\mathbf{k}}[\ln(1-e^{-\beta\omega_{\mathbf{k}up}})+\ln(1-e^{-\beta\omega_{\mathbf{k}vp}})] \tag{52}$$

where $E_p^0=\frac{1}{4}\sum_{\mathbf{k}\xi}\omega_{\mathbf{k}\xi p}$ is the quantum-mechanical zero-point energy.

The last term is the familiar entropy contribution,[17] $-T\mathcal{S}$, from bosonlike, transverse spin-wave excitations. At low temperature the energy and entropy contribution from the *longitudinal fluctuations* is negligible. Then the internal energy for $p=1$ and 2 [averaging the q dependence of $R^{\alpha}_{\mathbf{q}\xi p}(\sim R^{\alpha}_{p})$, which was added in Eq. (51) in order to cancel $\chi^{\alpha}_{\mathbf{q}\xi p}$ in Eq. (49)] can be written

$$E_1(T)=-2KM_1^2+D\langle S_z^2\rangle_1-\tfrac{1}{2}(R^x_1\langle S_x^2\rangle_1+R^y_1\langle S_y^2\rangle_1)\ , \tag{53}$$

$$E_2(T)=-2JM_2^2+D\langle S_z^2\rangle_2-\tfrac{1}{2}(R^z_2\langle S_z^2\rangle_2+R^y_2\langle S_y^2\rangle_2)\ .$$

The last terms are the energy contributions from the transverse excitations. They have the form of a Landau expansion for the local *transverse fluctuations*, with coefficients equal to minus one half of the inverse renormalized susceptibilities R^{α}_{0p} from Eqs. (46) and (47). At low temperatures, when the order parameter is close to the maximum value, the transverse correction is clearly small and the phase boundary is accurately given by the mean-field theory. At higher temperatures (or large D) the corrections become large, in particular close to the martensitic transition, where the short-range order of the competing phase become large. However, the correction gives to a first approximation the same contribution, $-k_BT$, for both phases, since $\langle S^2_{\alpha}\rangle\sim k_BT/R^{\alpha}_p$, and only corrections to this (equipartition result) shift the phase boundary. The entropy term, the last in Eq. (52), can become large if a mode goes soft. However, since we have shown this does not happen, the entropy term is not expected to shift the boundary significantly, either. The conclusion is that the *explicit* energy and entropy contributions from the transverse excitations do not "drive" the martensitic transformation, i.e., determine the first-order boundary. This is predominantly determined by the longitudinal contributions to the internal energy, the first two terms in Eq. (53). However, here the transverse mode plays a significant *implicit* role in the calculation of the thermal averages M_p and $\langle S_z^2\rangle_p$. This amounts to a renormalization of the temperature scale such that the order parameter M_p vanishes at a temperature T_{cp} given by the renormalized R^{α}_p, instead of at the $T^{\mathrm{MF}}_{\mathrm{cp}}$, given by R^{α}_p from the mean-field or RPA theory. This temperature renormalization can be very large, in particular in two dimensions. We expect the expressions for the free energy Eqs. (52) and (53) to be quite general, and consequently the conclusion should apply also to the classical case.

Let us now discuss the real structural martensitic transformation in the light of these results. In the model we allow the atoms to perform large-amplitude collective oscillations with each atom confined to a given surface (sphere). The response function Eq. (48) has precisely the form expected for renormalized phonons,[17] where the U and V modes correspond to the acoustic and optic modes and the α index denotes the two degrees of freedom for motions on the sphere. Vibrations perpendicular to the surface are assumed to have high frequencies and will therefore not have significant effects on the temperature dependence of the free energy. However, the large-amplitude motions on the surface result in strains in the crystal. A uniform strain ϵ_1 corresponding to M_1 and an internal strain ϵ_2 corresponding to M_2. The internal en-

ergy of the two phases [first terms in Eq. (53)] therefore depends on temperature and this mainly determines the martensitic phase boundary. This mechanism is sufficient. The entropy of the two phases [last term in Eq. (52)] is presumably quite similar and is not a determining "driving force" for the transition unless (a) one phase has a much softer mode than the other (Zener's mechanism[18]) or (b) the whole spectrum of frequencies $\omega_{k\xi p}$ is significantly smaller for one phase than the other (Friedel's mechanism[19]). The maximum frequencies are at $K=1.5J$ and $D=2J$, from Eqs. (34) and (42), $\omega_1(\max)=4JM_1$ and $\omega_2(\max)=4.9JM_2$ for $S=1$, whereas for the classical case at $K=2J$ one finds $\omega_1(\max)=4JM_1$ and $\omega_2(\max)=5.7JM_2$. Although the difference is small, $\omega_1(\max)$ is indeed smaller than $\omega_2(\max)$, as assumed by Friedel. Consequently the entropy $S_1>S_2$ and the larger cubic entropy tend to stabilize the cubic structure at high temperature, i.e., push the phase boundary to a lower K/J ratio. From this we conclude that the internal strain energies are most important, and Friedel's mechanism (b) is assisting, whereas the soft-mode (Zener) mechanism (a) is not decisive, for our model at least. Nonetheless let us discuss the soft-mode aspect a bit further since this has been the subject of several experimental efforts.[1,2,5]

F. Dynamical response function near a soft-mode transition

In the preceding sections we have shown that the first moment, say ω_{qup} in Eq. (48), of the response function Eq. (23) does soften considerably, although not completely, when approaching the weak first-order transition. If the spectrum was of the quasiharmonic form Eq. (48), this would imply that the observable excitation frequency, ω_{peak}, should also soften. This argument is the basis for the often discussed, expected soft-mode behavior at a martensitic transformation. However, when the first moment gets softer (or equivalently the susceptibility increases) it is clear from Eq. (49) that the short-range correlations increase. This makes the combined correlation functions Eq. (46), which enter in the excess second moment Δ_q^2 in Eq. (45), increase. A decreasing first moment, or an expected-soft-mode transition, is therefore invariably accompanied by a change in the dynamical line shape away from the simple δ-function spectrum Eq. (48). Whereas Eq. (48), using an accurate first moment frequency gives a good approximation for thermodynamic functions, which are integrated over frequency, this first moment is not to be identified with observed peak frequency. It is clear from Eq. (23) that the line-shape correction $\underline{\Sigma}_q(z)$, which is proportional to $\underline{\Delta}_q^2$, must be included when the excess moment grows large. In a simplest approximation, we use in the correlation theory the form

$$\underline{\Sigma}_q(z)=\underline{\Delta}_q^2/(z\underline{1}+\underline{K}) ,$$

which means that the random force correlation $(\underline{X}_q\underline{X}^{\dagger}{}_q)_z$ is supposed to decay exponentially—we call this a two-pole approximation because in the case of a single dynamical variable (i.e., no matrices) a response would be described by just two poles. Now for two or more dynamical variables the response will be described by twice the number of poles. It has been discussed previously, both for the $S=1$ singlet-doublet model[20] and for the antiferromagnet model,[21] that close to the expected soft-mode transition the spectrum for two dynamical variables has four complex poles, with the two complex poles at $\omega=\pm\alpha_1+i\beta_1$, with the real part larger than the first frequency $|\alpha_1|>\omega_{qup}$ Eq. (48), and two complex poles at $\omega=\pm\alpha_2+i\beta_2$, with a very small real part $|\alpha_2|\approx 0$, which appear as a central peak in the spectrum Eq. (48). The response at the frequency ω_{qup}, which is sharp for small Δ_q^2, will therefore renormalize to higher frequencies $\omega_{peak}=\pm\alpha_1+i\beta_1$ and simultaneously broaden when Δ_q^2 grows, and furthermore a response develops at low frequencies. The observed peak frequency ω_{peak} is therefore not expected to go soft. Now the intensity of the central peak is proportional to Δ_q^2 and inversely proportional to the first moment frequency. This intensity is therefore expected to grow strongly relative to the intensity of the peaks, since the total intensity is constant. The width and intensity of the central peak can be calculated self-consistently using the mode-mode coupling theory. This is shown in Fig. 3. However, in this theory only the correlation effects of two simultaneous excitations on neighboring sites are considered. The intensity grows because the probability for this to happen grows when there are many excitations in the system. This picture covers of course only the very beginning of spontaneous nucleations of the competing order corresponding to the excitations. The width is therefore usually found to be much larger than observed experimentally. The physical interpretation of the central peak is that it is the response of the nucleating clusters. The mode-mode coupling considers only clusters of two, whereas the experiments monitor much larger clusters, which have

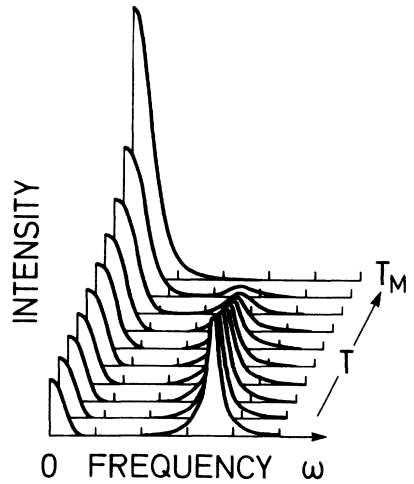

FIG. 3. The typical normalized dynamical response predicted by the correlation theory, showing that the finite frequency excitations (corresponding to phonons) do not soften, when approaching the martensitic transformation T_M, but loose intensity to a central peak, describing the time evolution of minority domains.

slower dynamics—and therefore give a more narrow central peak. However, the interesting result of the correlation theory is that, theoretically, spontaneous nucleation is predicted to occur. Nucleation stimulated by imperfections of one kind or another may of course in a practical situation dominate the physics. It is therefore important that by Monte Carlo computer simulation we can "experimentally" study a perfect case and, indeed, find spontaneous nucleation occurring. The discussed theory is for a system in thermodynamical equilibrium, and applies close to the transition region. However, with the simulation technique we can further study quenches to far from equilibrium situations and follow the kinetics of the domain growth. This will be discussed in the next section.

V. COMPUTER SIMULATION OF THE MARTENSITIC TRANSITION

Simulation of structural phase transitions by means of a lattice spin model, Eq. (1), circumvents many of the problems which are related to the boundary conditions in molecular dynamics calculations of nonlattice models.[22–25] The two types of ordered structures can be hosted within the same unit cell. Furthermore, the details of the transition can be studied in more detail by lattice model simulations since such simulations are practicable for larger systems. This fact has been used before to study structural phase transitions by means of ϕ^4-lattice models.[26,27] In particular, by means of the Monte Carlo method[28] it is possible to study nonequilibrium aspects of the phase transition[29] in relation to nucleation events and responses to rapid changes in the thermodynamic conditions.

A. Monte Carlo techniques for spin lattices

A general review of computer simulation techniques devised to study phase transitions in lattice spin models is given in Ref. 28. For the present model, Eq. (1), we have used conventional Monte Carlo importance sampling built on a stochastic Glauber-type single-site spin excitation mechanism by which the individual classical spin vectors are rotated through a random angle (rotational diffusion). Although the model Hamiltonian in Eq. (1) has its own nontrivial deterministic dynamics, we have imposed the more artificial Glauber dynamics in order to facilitate a careful study of the phase transition region, as well as an investigation of responses to rapid temperature changes. Molecular dynamics calculations exploiting the true dynamics will not be feasible for such purposes. Despite the artificial Glauber dynamics, the temporal evolution of the spin system towards thermal equilibrium after a change in the temperature will still mimic the kinetics of the spin model to the extent that the elementary excitations may be considered as composed of single-spin rotations. The time scale of these dynamics is then given in units of attempted Monte Carlo steps per site (MCS/S).

The simulations are carried out on finite lattices subject to the toroidal periodic boundary conditions. Effects due to finite size[28] are assessed by a systematic study of a series of different lattice sizes, $N=20^2$, 30^2, 40^2, 60^2, and 100^2. The statistical ensembles incorporate from 10^3 to 10^4 microconfigurations, depending on temperature. The systematics of the calculations for each set of values of the model parameters in Eq. (1) are as follows: Scans of increasing and decreasing series of temperatures and coupling constant ratios K/J are performed for systems initiated in the uniformly ordered triangular or quadratic phases, as well as in the disordered phase, in order to detect possible metastable behavior and hysteresis associated with the phase transformations. Some thermal quenches are performed in the neighborhood of the structural transition by suddenly changing the temperature across the transition. Similar quenches are performed from the disordered phase deep into either of the two ordered phases.

B. Energy, order parameters, and phase diagrams

The phase diagram of the $S=\infty$ model, Fig. 4, as spanned by the coupling-constant ratio K/J and temperature is derived from the behavior of the total internal energy, $E=\langle \mathcal{H} \rangle /N$, and the order parameter M, as well as the corresponding response quantities, i.e., specific heat and ordering susceptibility, as derived from the fluctuation theorem. The order parameter is defined as that component of the order-parameter vector

$$M_\alpha(T)=N^{-1}\left\langle \sum_{i=1}^{N} S_{i\alpha} e^{i\mathbf{q}_\alpha\cdot\mathbf{r}_i} \right\rangle, \quad \alpha=x,y,z \tag{54}$$

in which—in equilibrium—the actual long-range order resides. For ferromagnetic order ($n=1$), $\mathbf{q}_\alpha=\mathbf{q}_z=\mathbf{0}$, and for antiferromagnetic order ($n=2$), $\mathbf{q}_\alpha=\mathbf{q}_x=\pi/r_0(1,0)$ or $\mathbf{q}_\alpha=\mathbf{q}_y=\pi/r_0(0,1)$ where r_0 is the lattice parameter.

Selected scans of E and M along paths of constant K/J or temperature are shown in Figs. 5–7, which clearly signal the occurrence of phase transitions. The order of these phase transitions is determined by standard techniques[28] that involve a systematic study of the finite-size

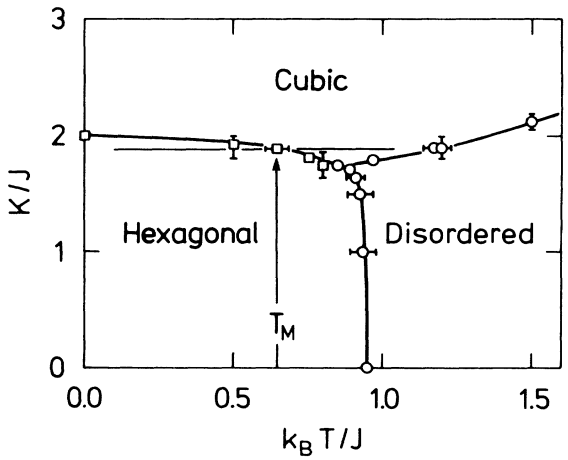

FIG. 4. Phase diagram spanned by coupling-constant ratio K/J and temperature for the $S=\infty$ model of Eq. (1) with $D=2J$. The results are obtained from Monte Carlo simulations. The cubic phase is the $n=1$ ferromagnetic phase and the hexagonal phase is the $n=2$ antiferromagnetic phase. First-order transitions are indicated by □ and continuous transitions by ○.

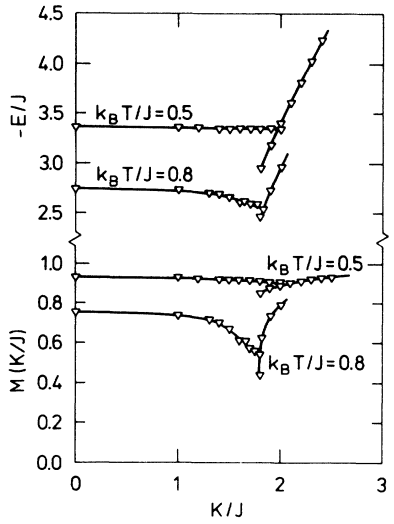

FIG. 5. Energy, E, and order parameter, M as functions of coupling-constant ratio, K/J, for selected values of the temperature. Monte Carlo results are shown for a system with $N=400$ spins and $D=2J$, Eq. (1). For increasing K/J, the system passes through a first-order transition from an antiferromagnetic to a ferromagnetic phase, cf. Fig. 4.

effects also seen on Figs. 6 and 7. The resulting phase diagram for $D=2J$ is shown in Fig. 4. Similar phase diagrams have been derived for other values of D. The diagrams consist of a first-order line separating the two ordered phases and two lines of continuous transitions

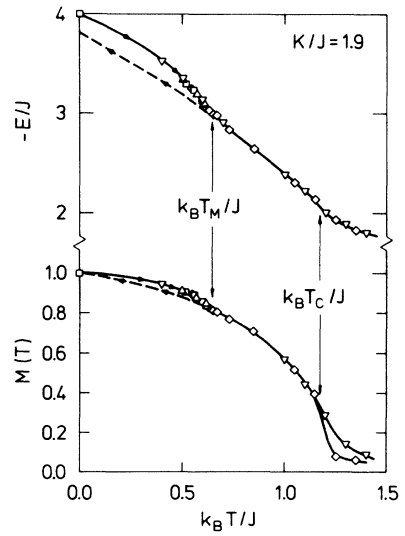

FIG. 6. Energy, $E(T)$, and order parameter, $M(T)$, as functions of temperature for $K/J=1.9$ and $D=2J$, Eq. (1). Data are obtained from Monte Carlo calculations on systems with N spins, ∇: $N=400$, ◇: $N=900$, △: $N=1600$, □: $N=3600$, and ○: $N=10000$. For increasing temperature, the system passes through two consecutive transitions, one of first order at T_M from the antiferromagnetic to the ferromagnetic phase and a continuous one at T_c from the ferromagnetic to the disordered phase, cf. Fig. 4. The dashed lines indicate a metastable path of supercooling the ferromagnetic phase.

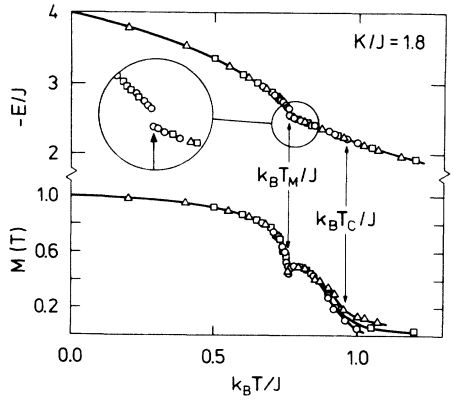

FIG. 7. Same as Fig. 6, except for $K/J=1.8$.

separating the ordered phases from the disordered one. The three lines meet in a bicritical point of a conventional type.[30] The first-order line of structural transitions is seen to be nonhorizontal, exposing the bicritical region as a region where the antiferromagnetic phase is suppressed. This suppression is enhanced when the value of D is increased. It is this suppression which furnishes the spin model proposed in the present paper with thermally driven structural transitions and, among other things, makes it a suitable candidate for modeling martensitic transformations.

Obviously, as K/J is decreased towards its bicritical value, the thermal range of the intermediate ferromagnetic phase is diminished and becomes more difficult to establish accurately by numerical simulations. Progressively larger systems have then to be simulated. It is interesting to note, cf. Fig. 7, that the order parameter in the intermediate phase is nonmonotonic in temperature, an effect which is clearly induced by fluctuations not accounted for in the mean-field theory.

The equilibrium data in Figs. 6 and 7 near the structural transition are obtained by approaching the transition region from both sides using systems with the pertinent uniform global ordering. Attempts to cross the transition region and generate new equilibrium order out of the old order proved not to be possible within reasonable times ($\lesssim 10^4$ MCS/S), except for the smallest systems which, however, seriously smear the transition. The extremely slow kinetics of the structural transition is discussed in Sec. V D. The kinetics of the thermal transitions becomes slower for larger values of K/J at which the crossing of the phase boundary occurs more tangentially. The dashed curves in Fig. 6 show a striking effect of this behavior: the ferromagnetic phase for $K/J=1.9$ can be retained as metastable all the way down to zero temperature.

C. Fluctuations and correlation length of short-range order

A detailed study of the equilibrium fluctuation effects accompanying the thermally induced structural transition at T_M has been conducted for a selected value of the coupling ratio, $K/J=1.8$; cf. Fig. 7. A qualitative representation of the correlated spin fluctuations is provided

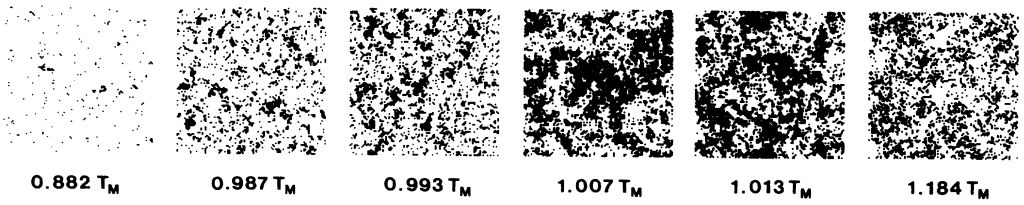

FIG. 8. Snapshots of minority-phase clusters in the vicinity of the structural transition at T_M, for $K/J=1.8$; cf. Fig. 7. Below T_M, the black dots indicate spins with predominantly ferromagnetic order, and above T_M, the black dots indicate predominantly antiferromagnetic order.

by Fig. 8, which shows typical snapshots of the cluster distributions of the minority domains in the two phases in the vicinity of T_M. In this figure, the nuclei of "opposite" order are pictured by black patches and dots, i.e., the black patches indicate spins which for $T<T_M$ are predominantly ferromagnetically ordered and for $T>T_M$ predominantly antiferromagnetically ordered. The criterion used to determine whether individual spins at a given temperature participate in a given type of ordering is chosen (somewhat arbitrarily) to be $|S_{i\alpha}|\geq M_\alpha(T)$. The snapshots of Fig. 8 clearly show that the "opposite" phase is nucleated very extensively near the structural phase transition, despite the fact that the two phases are not symmetry connected. The fluctuating clusters bear some resemblance to the fluctuations in long-range order near a critical point.[31,32]

A quantitative measure of the correlation length of short-range order is obtained via the first two moments

$$k_m^\alpha=\sum_q{}' |q-q_\alpha|^m\langle S_q^\alpha S_{-q}^\alpha\rangle \Big/ \sum_q{}' \langle S_q^\alpha S_{-q}^\alpha\rangle, \quad m=1,2 \tag{55}$$

of the static correlation function

$$\langle S_{\mathbf{q}}^\alpha S_{-\mathbf{q}}^\alpha\rangle = N^{-1}\left\langle \left| \sum_{j=1}^{N} S_{j\alpha} e^{i\mathbf{q}\mathbf{r}_j} \right|^2 \right\rangle , \tag{56}$$

where

$$q=2\pi j/\sqrt{N}, \quad j=-\sqrt{N}/2,\ldots,0,\ldots,\sqrt{N}/2 .$$

The primed sums of Eq. (55) are restricted by an ultraviolet cutoff, $|q|\leq Q$. From k_1^α and k_2^α, the correlation lengths of short-range order, ξ_α in units of 2π times the lattice constant, may be derived by the following approximate procedure. We assume that the correlation function is of Lorentzian form

$$\langle S_q^\alpha S_{-q}^\alpha\rangle = \frac{C}{\xi_\alpha^{-2}+q^2} \quad \text{for } |\mathbf{q}|<Q , \tag{57}$$

where C is a constant. The first two moments are then given by

$$k_1^\alpha = 2[Q-\xi_\alpha^{-1}\arctan(Q\xi_\alpha)]/\ln\Gamma \tag{58}$$

and

$$k_2^\alpha = (Q^2-\xi_\alpha^{-1}\ln\Gamma)/\ln\Gamma \tag{59}$$

with

$$\Gamma = 1+Q^2\xi_\alpha^2 . \tag{60}$$

It then follows, in the limit $Q\xi_\alpha\gg 1$, that the correlation-length is given by

$$\xi_\alpha \simeq \frac{k_1^\alpha}{2k_2^\alpha}\exp[2k_2^\alpha/(k_1^\alpha)^2] . \tag{61}$$

In Fig. 9 are given the Monte Carlo results for certain powers of the first two moments of the correlation function of short-range order, Eq. (57), i.e., of the ordering "opposite" to that of the equilibrium ordering in the host phase. These powers are chosen in order to associate the moments with dimensions of length. Both $(k_1^\alpha)^{-1}$ and $(k_2^\alpha)^{-1/2}$ have a pronounced peak at the structural transition. The position and intensity of the peak are found, within the numerical accuracy, to be the same for the two larger systems, thus indicating that the correlations contributions to k_1^α and k_2^α are not seriously invalidated by finite-size effects. The numerical accuracy is not sufficient to resolve a possible discontinuity in the two

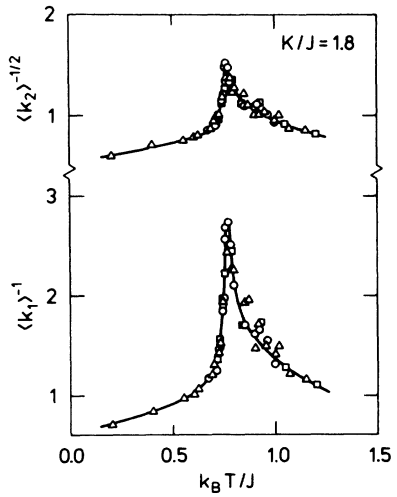

FIG. 9. Powers of first and second moments of the correlation function of short-range order, Eqs. (55) and (56), as functions of temperature in the vicinity of the structural phase transition at T_M. The data are derived from Monte Carlo calculations on systems of different sizes; cf. the caption to Fig. 6, in the case $K/J=1.8$.

moments at T_M. The large scatter in the data for different system sizes found in the high-temperature wing of the graphs in Fig. 9 is due to crossing the critical line in the phase diagram, cf. Figs. 4 and 7. There are no indications of a critical anomaly in k_1^α or k_2^α at T_c, however. The correlation length derived from the data displayed in Fig. 9 using Eq. (61) is shown in Fig. 10, which substantiates quantitatively the observation from Fig. 8 that the correlation of short-range order increases very dramatically approaching T_M from both sides. The spin density fluctuations are thus very strong, although finite, at the structural transition. This behavior bears some resemblance to pseudocritical behavior.[32] For larger values of K/J, ξ_α retains its sharp peak, although with less intensity. There is an overall asymmetry in ξ_α as seen in Fig. 10. The larger values of ξ_α above T_M may to some extent be caused by the proximity of the critical line. In the immediate vicinity of T_M, there are, however, no indications of any pronounced asymmetry. The apparent difference in cluster sizes seen in Fig. 8 for $T=0.993\ T_M$ and $T=1.007 T_M$ is simply caused by a visual coalescence of degenerate x and y clusters in the ferromagnetic phase. In fact, it is found semiquantitatively that the cluster density at $T=1.007 T_M$ is about twice that at $T=0.993 T_M$. A quantitative analysis of the cluster distribution functions similar to that of Ref. 33 is not feasible for the present model due to the ambiguity associated with defining the borders of the clusters in a strongly fluctuating system with continuous site variables.[34]

D. Kinetics of first-order structural transitions

The kinetics of the ordering processes involved in the structural transiton has been studied numerically by several types of simulated thermal quenches across T_M. The kinetics of the structural transition is particularly interesting since it involves competition between two different ordering processes of different symmetry.

The Monte Carlo temperature quenches from T_i to T_f are performed globally by initiating the system in a spin configuration, which is typical of the temperature T_i. The system is then at time $t=0$ subject to instant cooling or heating by assigning the new temperature, T_f, to the heat bath to which the spin system is coupled. A global temperature quench provides a time series of spin configurations, each of which is characterized by a domain distribution. A number of quantities can be used to monitor quantitatively the growth of ordered domains as time lapses.[28] We shall here use (a) the length scale measures derived from the moments of the dynamical correlation function $\langle S_q^\alpha(t) S_{-q}^\alpha(t)\rangle$, i.e., $[k_m^\alpha(t)]^{-1/m}$, cf. Eqs. (55) and (56), and (b) the excess internal energy $\Delta E(t)=E(t)-E(T_f)$, where $E(T_f)$ is the equilibrium energy at T_f. $\Delta E(t)$ is a measure of the nonequilibrium energy associated with the entire domain-boundary network which forms spontaneously after the quench is initiated. The domain-growth kinetics is usually analyzed in terms of simple powers laws,

$$l_m^\alpha(t)\equiv[k_m^\alpha(t)]^{-1/m}-[k_m^\alpha(t=0)]^{-1/m}\sim t^{n_l} \tag{62}$$

and

$$\Delta E(t)\sim t^{-n_E}\ . \tag{63}$$

Dynamical scaling would imply that the two growth exponents are identical.[35] Regarding technical details concerned with the handling of structure factors of inhomogeneous systems and the finite-size symmetry breaking in systems with degenerate order parameters, the reader is referred to Refs. 36 and 37. Here, we give the main results of our simulated quenches.

The following types of quenches have been performed: deep down temperature quenches, (i) $T_i=\infty\rightarrow T_f=0$ and (ii) $T_i=1.03 T_M\rightarrow T_f=0$; and quenches within the transition region, (iii) $T_i=1.03 T_M\rightarrow T_f=0.97 T_M$ and (iv) $T_i=0.97 T_M\rightarrow T_f=1.03 T_M$. In Fig. 11 are shown the re-

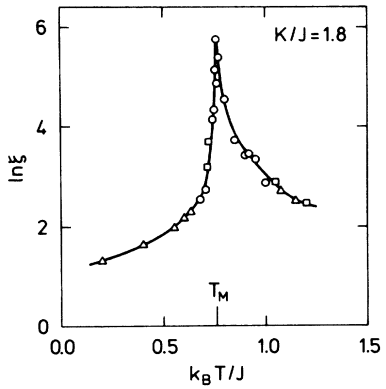

FIG. 10. Correlation length of short-range order, ξ_α, Eq. (61), shown in a semilog plot as a function of temperature in the vicinity of the structural phase transition. For clarity, only large-system data representing the thermodynamic limit are displayed in this figure: $K/J=1.8$.

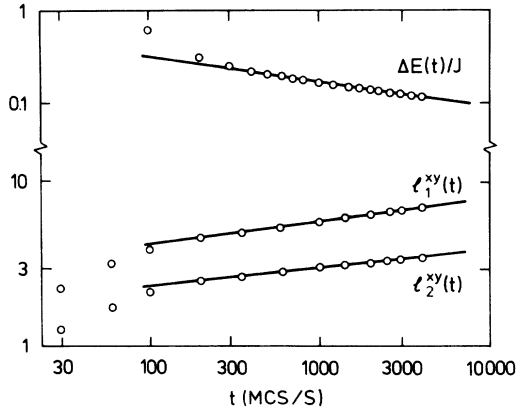

FIG. 11. Log-log plot vs time of length scales $l_m^{xy}(t)=\frac{1}{2}[l_m^{(t)}+l_m^{y}(t)]$, Eq. (62), and excess energy $\Delta E(t)$, Eq. (63), for a deep down temperature quench, $T_i=1.03 T_M\rightarrow T_f=0$, simulated on a lattice with $N=100^2$ spins. The time is measured in units of MCS/S. The solid lines denote asymptotic growth laws, Eqs. (62) and (63), with a common growth exponent $n\simeq 0.13\pm 0.03$.

sults for the simulated domain-growth kinetics in an $N=100^2$ system subject to a quench of type (ii). During this quench, the equilibrium clusters of the antiferromagnetic minority domains seen in Fig. 8 [with finite values of $k_m^\alpha(t=0)$, cf Eq. (62)], act as nucleation centers for antiferromagnetic domains. There are four thermodynamically equivalent antiferromagnetic domains which, during their growth processes, will mutually compete in their attempt to destroy the ferromagnetic order. The domain growth process has been followed up to $\simeq 4000$ MCS/S, beyond which finite-size effects come seriously into play: the extent of the four types of order is no longer approximately the same and the largest domains have sizes comparable to that of the entire system. It is noted that the antiferromagnetic domains actually grow at zero temperature. Figure 11 demonstrates that the growth kinetics is accurately described by the power laws in Eqs. (62) and (63) for $t \geq 200$ MCS/S. Furthermore, all three quantities are characterized by the same growth exponent

$$n \simeq n_E \simeq n_l \simeq 0.13 \pm 0.03 \ .$$

The value of the growth exponent is very low and thus the formation of the uniform antiferromagnetic phase from the ferromagnetic phase is a very slow process.

The growth after a deep quench was recently studied in a similar model as Eq. (1), but restricted to only two equivalent antiferromagnetic domains.[38] Here one finds the growth exponent $n \sim \frac{1}{4}$. The slow growth was analyzed and found to be due to a time dependent self-pinning. It is possible that there are additional topological pinnings operating in the present unrestricted four domain models, which further slows down the growth. This is currently under further investigation.[39]

The other deep quench (i) takes the system all the way from the disordered phase to the antiferromagnetic phase by crossing two phase transitions and the intermediate ferromagnetic phase. It is found that during the early time regime $t \leq 1000$ MCS/S, antiferromagnetic as well as ferromagnetic domains are formed and mutually compete. In this regime, the length scales of all six types of domains, $[k_m^\alpha(t)]^{-1/m}$, $\alpha = x,y,z$ obey simple growth laws with the same exponent whose value is again around 0.13. For $t \geq 1000$ MCS/S, the correlation length of the ferromagnetic domains starts to decrease, whereas the antiferromagnetic domains grow steadily.

The results of the quenches (iii) and (iv) within the structural transition region are less conclusive. In analogy with findings for other models quenched into transition regions, in particular close to critical points,[35] we find that the fluctuations near T_M slow down the growth, and the effective exponent value becomes very small. Our data are insufficient to sustain a quantitative analysis of the growth in this region.

VI. DISCUSSION

We have constructed a magnetic analog model of a displacive first-order structural transition. Thereby one can effectively model and focus the attention on the most relevant large amplitude vibrations the atoms perform during the displacements. For description of a displacive phase transition even a very sophisticated self-consistent phonon theory is of limited applicability. An advantage of a spin model is that a theory can be developed for large-amplitude vibrations. Furthermore, consideration of only the limited, most relevant atomic motions as modeled by the spin model, makes computer simulation of the transition much simpler than a full molecular dynamics calculation including all the possible atomic movements. The analysis of the model shows that the martensitic transformation within this model belongs to the problem of an ordinary bicritical point phase diagram with a weak first-order transition line, terminating as a function of temperature at a bicritical point. The interest here is in what happens along the line. Comparing the mean-field phase diagram with the two-dimensional Monte Carlo results for classical spin shows agreement at $T=0$, but expected very large temperature renormalization, reducing the temperature scale by as much as 60%, and some further modifications close to the bicritical point. The important conclusion is that correlation effects play a significant role determining the phase line. In the classical spin case the transition is in simple, linear theories as well as in the simulation found to be of first order and possible as a function of temperature without soft modes. The theory for the quantum $S=1$ model shows that this model is much more sensitive to the accuracy of the theoretical treatment. Thus in simple linear theories, the transition is of first order and simultaneously accompanied by a soft mode when approaching from both ordered phases and with a temperature independent phase line (in mean-field theory). The linear theory corresponds to harmonic phonon theory. This exemplifies clearly that a phenomenon as a martensitic transformation cannot be described by simple linear (small-amplitude) theory. With nonlinear effects taken into account, the $S=1$ model exhibits a martensitic transformation versus temperature, and exemplifies the case where the cubic structure is unstable at low temperatures, but is stabilized by large-amplitude vibrations at high temperature. This is a situation which is probably very common in the displacive double-well transition problem[8]—and definitely found in Zr.[4] The calculation shows that the transition is weakly[4] first order and the susceptibility of the competing order is growing when approaching the transition. This implies that the first frequency moment of the dynamical response decreases (softens) although not completely, simultaneously with increase of the short-range order. The latter has been directly observed in the Monte Carlo simulations. Because of the large-amplitude vibrations the resonances in frequency spectrum not only renormalizes to higher frequencies, but simultaneously a central peak develops. This is associated with the dynamics of the dynamically nucleating clusters. In the theory only the initial effect of the simultaneous displacement of two neighboring atoms is considered in the simplest mode-mode coupling approximation. The pair can fluctuate or move relatively fast and therefore gives a broad central peak. Experiments are dominated by the behavior of larger clusters, which move slower and consequently give a sharper central peak. The computer simulation shows that the ordered phase indeed grows

out of the thermally created fluctuations of the minority phase close to the phase separation line. This is a spontaneous nucleation process very similar to the critical fluctuations near a continuous phase transition.

All these phenomena therefore shows that precursor effects are indeed expected at the martensitic transformation. In our model we have not included long-range interactions, like the strain in real systems. These have the symmetry of the dipole interaction and would give rise to rather anisotropic clusters. This can be modeled in a simple fashion by increasing the anisotropy parameter P (here chosen as $2J$). When this is done[38] one finds domain boundaries dominated by stacking fault boundaries between twins.

The Monte Carlo simulation results confirm the theoretical predictions for the equilibrium properties near the transition. However, it also allows a study of the far-from-equilibrium behavior in a quench from one ordered phase to another. The kinetics of the domain growth is found to be algebraic t^{-n}, but with an exceedingly small exponent $n \sim 0.13$. This is well outside any of the expected universality classes with $n = \frac{1}{2}$ or $\frac{1}{3}$. The slow behavior is probably due to pinning effects of the simultaneously growing equivalent domains. This is analyzed further in a subsequent paper.[39]

ACKNOWLEDGMENTS

This work was supported by the Danish Natural Science Research Council under Grant Nos. 11-5176 and 5.21.99.72.

[1]Z. Nishiyama, *Martensitic Transformations* (Academic, New York, 1978); *Phase Transformations in Solids,* Materials Research Society Symposia Proceedings **21**, Crete, 1983, edited by T. Tsakalakos (North Holland, New York, 1984). For computer simulation and theory see S. Wen, J. W. Morris, and A. G. Khachaturyan, in Proceedings of the International Conference on Martensitic Transformations, Cambridge, Mass., 1979 (unpublished), p. 94; A. G. Khachaturyan, *Theory of Structural Transformations in Solids* (Wiley, New York, 1983). A recent experimental investigation is by O. Blaschko, G. Krexner, J. Pleschiutschnig, G. Ernst, C. Hitzenberger, H. P. Karnthaler, and A. Korner, Phys. Rev. Lett. **60**. 2800 (1988).

[2]J. A. Krumhansl, *Nonlinearity in Condensed Matter,* Vol. 69 of *Springer Series in Solid State Sciences,* edited by A. R. Bishop, D. K. Cambell, S. E. Trudlinger, and P. Qumar (Springer-Verlag, New York, 1987), p. 255; G. R. Barsch, J. A. Krumhansl, L. E. Tanner, M. Wuttig, Scripta Metall. **21**, 1257 (1987); D. Silberstein and P. C. Clapp, Phys. Rev. B **38**, 9555 (1988); J. A. Krumhansl and R. J. Gooding, *ibid.* **39**, 3047 (1989).

[3]P.-A. Lindgård and O. G. Mouritsen, Phys. Rev. Lett. **57**, 2458 (1986).

[4]Y.-Y. Ye, Y. Chen, K.-M. Ho, B. N. Harmon, and P.-A. Lindgård, Phys. Rev. Lett. **58**, 1769 (1987).

[5]C. Stassis, J. Zarestky, D. Arch, O. D. McMasters, and B. N. Harmon, Phys. Rev. B **18**, 2632 (1978); C. Stassis, J. Zarestky, and N. Wakabayashi, Phys. Rev. Lett. **41**, 1726 (1978); C. Stassis and J. Zarestky, Solid State Commun. **52**, 9 (1984).

[6]P. A. Lindgård, *Spin Waves and Magnetic Excitations,* edited by A. J. Borovik-Romanov and S. K. Sinha (North-Holland, New York, 1988), Vol. 22.1, Chap. 5; P.-A. Lindgård, Phys. Rev. **30**, 2729 (1984).

[7]J. Yeomans, Solid State Phys. **41**, 151 (1988).

[8]A. I. Larkin and V. G. Vaks, Zh. Eksp. Teor. Fiz. **49**, 975 (1965) [Sov. Phys.—JETP **22**, 678 (1966)]; A. I. Larkin and S. A. Pipin, *ibid.* **56**, 1664 (1969); [*ibid.* **29**, 891 (1969)]; G. A. Gehring and K. A. Gehring, Rep. Prog. Phys. **38**, 1 (1975).

[9]G. C. Wang and T. M. Lu, Phys. Rev. Lett. **50**, 2014 (1983).

[10]T. Hashimoto, T. Miyoshi, and H. Ohtsuke, Phys. Rev. B **13**, 1119 (1976).

[11]*Physical Properties and Thermodynamic Behavior of Minerals,* Vol. 225 of *NATO Advanced Study Institute, Series C,* edited by E. Sajle (Kluwer, Dordrecht, 1988).

[12]J. H. Van Vleck, *Electric and Magnetic Susceptibilities* (Oxford, London, 1932).

[13]T. Holstein and H. Primakoff, Phys. Rev. **58**, 1098 (1940).

[14]H. Mori, Prog. Theor. Phys. **33**, 423 (1965).

[15]P.-A. Lindgård and O. Danielsen, J. Phys. C **7**, 1523 (1974).

[16]S. K. Tyablikov, *Methods in Quantum Theory of Magnetism* (Plenum, New York, 1967).

[17]See D. C. Wallace, *Thermodynamics of Crystals* (Wiley, New York, 1972).

[18]C. Zener, Phys. Rev. **71**, 846 (1947).

[19]J. Friedel, J. Phys. Lett. (Paris) **35**, L59 (1974).

[20]P.-A. Lindgård, Phys. Rev. Lett. **50**, 690 (1983).

[21]P.-A. Lindgård, Phys. Rev. B **30**, 2729 (1984).

[22]T. Schneider and E. Stoll, Phys. Rev. Lett. **31**, 1254 (1973).

[23]P. C. Clapp and J. Rifkin, *Proceedings of the International Conference on Solid-State Phase Transformations,* edited by H. I. Aaronson *et al.* (The Metallurgical Society of AIME, Warrendale, Pa, 1982), p. 1165.

[24]J. R. Ray and A. Rahman, J. Chem. Phys. **80**, 4423 (1984).

[25]G. Delorenzi and C. P. Flynn, J. Phys. C **18**, L769 (1985).

[26]W. C. Kerr, Phys. Rev. B **19**, 5773 (1979); W. C. Kerr and A. R. Bishop, *ibid.* **34**, 6295 (1986).

[27]L. D. Roelofs, G. Y. Hu, and S. C. Ying, Phys. Rev. B **28**, 6369 (1983).

[28]O. G. Mouritsen, *Computer Studies of Phase Transitions and Critical Phenomena* (Springer, Heidelberg, 1984).

[29]J. D. Gunton, M. San Miguel, and P. S. Sahni, in *Phase Transitions and Critical Phenomena,* edited by C. Domb and J. Lebowitz (Academic, New York, 1983), Vol. 8, p. 267.

[30]M. E. Fisher and D. R. Nelson, Phys. Rev. Lett. **32**, 1350 (1974); J. M. Kosterlitz, D. R. Nelson, and M. E. Fisher, Phys. Rev. B **13**, 412 (1976).

[31]D. Stauffer, Phys. Rep. **54**, 1 (1979).

[32]H. Ikeda, Prog. Theor. Phys. **61**, 1023 (1979).

[33]O. G. Mouritsen and M. J. Zuckermann, Eur. Biophys. J. **12**, 75 (1985).

[34]See also O. G. Mouritsen, Phys. Rev. B **31**, 2613 (1985).

[35]A. Sadiq and K. Binder, J. Stat. Phys. **35**, 517 (1984).

[36]O. G. Mouritsen, Phys. Rev. Lett. **56**, 850 (1986); O. G. Mouritsen and E. Praestgaard, Phys. Rev. B **38**, 2703 (1988).

[37]J. Viñals and J. D. Gunton, Surf. Sci. **157**, 473 (1985).

[38]T. Castán and P.-A. Lindgård, Phys. Rev B **40**, 5069 (1989).

[39]T. Castán and P.-A. Lindgård (unpublished).

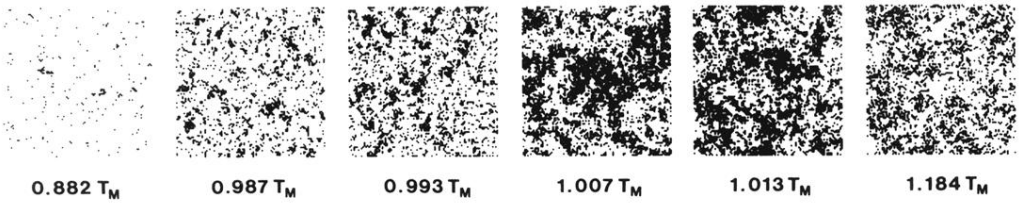

FIG. 8. Snapshots of minority-phase clusters in the vicinity of the structural transition at T_M, for $K/J = 1.8$; cf. Fig. 7. Below T_M, the black dots indicate spins with predominantly ferromagnetic order, and above T_M, the black dots indicate predominantly antiferromagnetic order.